IOPscience iopscience.iop.org

Home Search Collections Journals About Contact us My IOPscience

Spin transition in $[Fe(PM\text{-}BiA)_2(NCS)_2]$ studied by the electron paramagnetic resonance of the Mn^{2+} ion

This article has been downloaded from IOPscience. Please scroll down to see the full text article.

2000 J. Phys.: Condens. Matter 12 5481

(http://iopscience.iop.org/0953-8984/12/25/312)

View the table of contents for this issue, or go to the journal homepage for more

Download details:
IP Address: 171.66.16.221
The article was downloaded on 16/05/2010 at 05:16

Please note that terms and conditions apply.

J. Phys.: Condens. Matter **12** (2000) 5481–5494. Printed in the UK PII: S0953-8984(00)11591-7

Spin transition in $[Fe(PM\text{-}BiA)_2(NCS)_2]$ studied by the electron paramagnetic resonance of the Mn^{2+} ion

Hervé Daubric†, Janis Kliava†§, Philippe Guionneau‡, Daniel Chasseau‡, Jean-François Létard‡ and Olivier Kahn‡‖

† Centre de Physique Moléculaire Optique et Hertzienne, UMR Université Bordeaux I CNRS 5798, 351 cours de la Libération, 33405 Talence Cédex, France
‡ Laboratoire des Sciences Moléculaires, Institut de Chimie de la Matière Condensée de Bordeaux, UPR CNRS 9048, 33608 Pessac Cédex, France

E-mail: jkliava@frbdx11.cribx1.u-bordeaux.fr

Received 3 February 2000, in final form 25 April 2000

Abstract. The spin transition of Fe^{2+} ions in the mononuclear compound cis-bis(thiocyanato)-bis(N-2′-pyridylmethylene)-4-(aminobiphenyl)-iron(II) is studied by electron paramagnetic resonance (EPR) of Mn^{2+}. In cooling the compound down to the temperature range 174–168 K, the Fe^{2+} ions undergo a complete transition from the high spin (HS, $S = 2$) to the low spin (LS, $S = 0$) state, occurring with a narrow, ∼5 K and unusually sharp hysteresis loop. The temperature dependence of the unit cell parameters is almost linear on both sides of the spin transition; the variation of the unit cell parameters at the spin transition is very anisotropic. The EPR spectra, typical of the Mn^{2+} ion, only gradually change with temperature in the two spin states of Fe^{2+} but undergo a striking transformation in the spin transition range. This shows that a considerable cooperativity exists between the metal ions. Computer simulations using a laboratory-developed simulation program indicate significant changes in the zero-field splitting (zfs) parameters in the course of the spin transition. Lower-than-axial symmetry of the environment of Mn^{2+} persists in both spin states of Fe^{2+}; however, a stronger axial distortion arises in the HS state.

The temperature variations of the zfs parameter D are related to transformations of the crystal structure using the Newman superposition model amended for contributions of thermal expansion of the crystal lattice and lattice vibrations. Computer fits show a reduction of the model parameter—power law exponent—in the LS state, $t_2 = 4$, in comparison with the HS state, $t_2 = 8$. Such a tendency is consistent with the decrease of the Fe–N bond lengths in the HS to LS transition.

1. Introduction

The spin crossover exhibited by ferrous (Fe^{2+}, configuration $3d^6$) compounds has been extensively studied in the last three decades [1–10]. The main challenge offered by such materials is the possibility of their use in data processing, i.e. memory devices, storage displays [3, 4] and in nonlinear optical applications [5, 6]. The change of the electronic state of Fe^{2+} from high spin (HS, $S = 2$) to low spin (LS, $S = 0$) can be induced by a variation of temperature, pressure or by light irradiation. In solid state, if site-to-site interactions are strong enough, the spin conversion may become cooperative. This results in abrupt spin transitions with hysteresis, the critical temperature of the LS and HS conversion, $T_{1/2\uparrow}$, being higher than that of the HS to LS conversion, $T_{1/2\downarrow}$. Such spin-changing systems are bistable and possess a memory effect.

§ To whom correspondence should be addressed.
‖ Deceased.

 © 2000 IOP Publishing Ltd

The origin of this cooperativity still remains uncertain; indeed, fine chemical modifications can drastically modify the magnetic behaviour of spin-changing compounds. Particularly illustrative of this phenomenon is the family of ferrous compounds $[Fe(PM\text{-}L)_2(NCS)_2]$, based on 2′-pyridylmethylene 4-amino derivatives with different aryl units [7–9]. Despite their structural similarity, these compounds exhibit very different magnetic properties: from incomplete spin conversion to discontinuous transitions with hysteresis. For instance, $[Fe(PM\text{-}BiA)_2(NCS)_2]$ in phase I shows an unusually abrupt spin transition with a narrow hysteresis, $T_{1/2\downarrow} = 168$ K and $T_{1/2\uparrow} = 173$ K [8], while $[Fe(PM\text{-}PEA)_2(NCS)_2]$ presents a very large hysteresis, $T_{1/2\downarrow} = 194$ K and $T_{1/2\uparrow} = 231$ K [7]. Moreover, $[Fe(PM\text{-}BiA)_2(NCS)_2]$ in phase II, obtained with a different synthesis method, exhibits a complete and gradual spin conversion around 207 K [5]. Stacking of aromatic rings allows the formation of single crystals. Crystal structures of four $[Fe(PM\text{-}L)_2(NCS)_2]$ compounds, determined by x-ray diffraction, have been reported in both the HS and LS states [8, 9]. These data suggest that the strong cooperativity is related to the two-dimensional character of the crystal structure resulting from close contacts between aromatic rings belonging to adjacent molecules. Note that only in $[Fe(PM\text{-}PEA)_2(NCS)_2]$ the x-ray diffraction indicates that the spin transition is accompanied by a structural phase change. Our recent electron paramagnetic resonance (EPR) study of $[Fe(PM\text{-}PEA)_2(NCS)_2]$ doped with Mn^{2+} corroborates this conclusion; besides, it suggests that the spin transition occurs in domains of like-spin ions [10].

The Fe^{2+} ions are 'EPR silent' not only in the LS (diamagnetic) state, but usually in the HS (paramagnetic) state, as well (at least at elevated temperatures and in microwave bands), because of very short spin–lattice relaxation times and/or large zero-field splitting. Therefore, its spin conversion can be detected by EPR only in an *indirect way*, by doping the compound with foreign paramagnetic ions—spin probes. The EPR spectrum of a spin probe is modified in the course of the spin conversion experienced by the Fe^{2+} ions. Note that there can be two different causes of this modification: first, spin–spin interactions between the spin probe and Fe^{2+} in the (paramagnetic) HS state; second, a structural change accompanying the spin conversion. In the case of spin probes, the EPR spectra modifications caused by this structural change yield data not on (more or less trivial) *short-range* transformations in the environment of the Fe^{2+} ions but rather on *long-range* transformations involving the whole crystal structure.

Up to now, only three spin probes have been systematically used in the EPR studies of ferrous spin transition compounds, *viz*., Cu^{2+} ($3d^9$), Fe^{3+} and Mn^{2+} ($3d^5$) [10–21]. The latter ion is certainly the most promising one for this type of study, since its EPR spectra, exhibiting both zero-field splitting (zfs) and hyperfine splitting (hfs), provide more data on the local structure in comparison with other spin probes. Moreover, as Mn^{2+} has the $^6S_{5/2}$ ground state, no Jahn–Teller distortion occurs for this ion (this distortion may obscure structural inferences of the EPR data, as is the case with the Cu^{2+} probe [16, 17]).

The present work deals with the EPR of $[Fe(PM\text{-}BiA)_2(NCS)_2]$. Preliminary EPR [18] and x-ray powder diffraction studies [8] reveal that the phases I and II of this compound have totally different structures. Here we focus on the temperature dependence of the EPR spectra of the phase I (naturally doped with Mn^{2+} ions) in relationship with the temperature dependence of the unit cell parameters. The Newman superposition model [22] is applied in order to relate the zfs parameters with the crystal structure.

2. Sample preparation and experiment

$[Fe(PM\text{-}BiA)_2(NCS)_2]$ was prepared as previously described [8] and was found to be naturally doped with manganese ions. Indeed, the iron(II) sulphate heptahydrate used for the synthesis can contain up to 0.05% Mn/Fe. Elemental analysis performed by the Service Central

d'Analyse (CNRS) in Vernaison (France) has shown a doping level of ∼0.1% Mn/Fe. Analysis calculated for $Fe_{0.999}Mn_{0.001}C_{38}H_{28}N_6S_2$: C, 66.28; H, 4.07; N, 12.21; S, 9.30; Fe, 8.14. Found: C, 63.76; H, 4.08; N, 11.82; S, 9.38; Fe, 7.81; Mn, 0.008.

Very few single crystals of the title compound could be obtained. They looked like black plates of approximate dimension $0.50 \times 0.35 \times 0.10$ mm^3 and showed fragility towards x-ray irradiation in the spin transition range. Therefore, different crystals were used to determine the cell parameters from room temperature down to 170 K (in the HS state) and at 140 and 25 K (in the LS state). Diffraction experiments above the spin transition were carried out on a Nonius CAD-4 diffractometer equipped with a laboratory-made N2 open flow cryostat. The cell parameter variations (ten sets of data) were determined by cooling from 298 K to 174 K at a rate of 0.5 K min^{-1} with stopping points of ∼2 h to measure the cell parameters. The standard deviation of the temperature was about 3 K. The same 25 selected Bragg reflections were used for the different sets. Below the spin transition the cell parameters were measured with a Bruker SMART-CCD, with the same rate of cooling as previously. In all cases, 40 frames (20 seconds per frame) were recorded yielding more than 300 reflections.

The X-band ($\nu = 9.3$ GHz) EPR spectra in the 168–177 K range were recorded with a Varian V4502 spectrometer equipped with a Varian E257 variable temperature accessory and a numeric data recording unit. In the 20–70 K range a Bruker EMX spectrometer provided with an ER4112HV variable temperature unit was used. The Q-band ($\nu = 34$ GHz) EPR spectra were recorded in the 114–293 K range with a Bruker ESP300 spectrometer supplied with an ER4121VT digital temperature control unit.

3. Results

3.1. X-ray diffraction

The crystal structure of $[Fe(PM\text{-}BiA)_2(NCS)_2]$ in phase I, determined by x-ray diffraction at both 298 K (HS state) and 140 K (LS state), has been reported previously [8]. This compound crystallizes in the $Pccn$ space group at all temperatures in the two spin states. The molecular packing can be described as sheets of molecules parallel to the ac plane. In both spin states the Fe^{2+} ion lies on a twofold axis and is surrounded by three pairs of nitrogen atoms, the first one belonging to two NCS-groups in the *cis* position and the two remaining ones to two PM-BiA ligands. The spin transition induces a strong change in the environment of Fe^{2+}, *viz*., a dramatic reduction of the Fe–N bond lengths occurs in the LS state with respect to the HS state, $\Delta^{max}_{Fe-N} \sim 0.3$ Å. This is the largest bond length reduction observed up to now in ferrous spin transition compounds. Besides, the crystallographic data indicate that the FeN_6 core becomes more regular in the LS state, as all N–Fe–N angles converge to 90°.

Figure 1 shows that the unit cell parameters decrease almost linearly from room temperature to 174 K. Within the range 174–125 K a marked strongly anisotropic change takes place. Namely, in the HS to LS transition region the c parameter increases (∼4.0%) while a strongly decreases (∼4.5%) while b does not show a drop in its temperature dependence. The relative volume reduction over the whole transition range is ∼7.3% corresponding to the reduction rate of 0.93 Å^3 K^{-1}. A similar behaviour has previously been observed in other ferrous spin-crossover compounds; i.e. $Fe(PM\text{-}PEA)_2(NCS)_2$ [7], $Fe(btz)_2(NCS)_2$ [23] and $Fe(Phen)_2(NCS)_2$ [23].

From previous x-ray diffraction studies of molecular compounds one can conclude that in the absence of a phase transition the temperature dependence of the thermal expansion tensors is approximately linear [24, 25]. The results obtained with $[Fe(PM\text{-}BiA)_2(NCS)_2]$ also infer a linear temperature dependence of the unit cell parameters in the HS and LS regions.

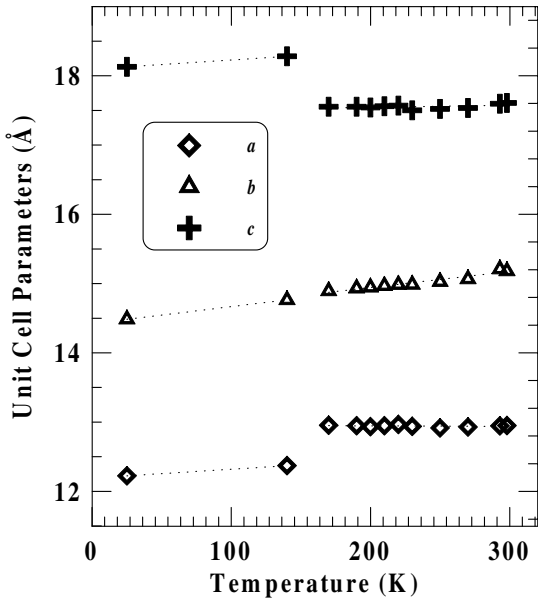

Figure 1. Temperature dependence of the unit cell parameters (symbols) and linear fits, see equation (1) (dashed curves) for $[Fe(PM\text{-}BiA)_2(NCS)_2]$ versus temperature. The fitting parameters are listed in table 1.

Table 1. Linear fit parameters of equation (1) for the LS and HS states of $[Fe(PM\text{-}BiA)_2(NCS)_2]$.

Fitting parameters	LS state	HS state
a_0 (Å)	12.192	12.962
α_a (10^{-3} K^{-1})	0.104	−0.006
b_0 (Å)	14.423	14.480
α_b (10^{-3} K^{-1})	0.169	0.160
c_0 (Å)	18.098	17.485
α_c (10^{-3} K^{-1})	0.072	0.017

Thus, the following relations can be used to fit the experimental temperature dependence of these parameters outside the spin transition region:

$$a(T) = a_0(1 + \alpha_a T) \qquad b(T) = b_0(1 + \alpha_b T) \qquad c(T) = c_0(1 + \alpha_c T) \quad (1)$$

where a_0, b_0 and c_0 are the zero-temperature unit cell parameters and α_a, α_b and α_c the corresponding thermal expansion coefficients. Table 1 summarizes the fitting parameters for the two spin states.

3.2. EPR spectra

The transformation of the EPR spectra in the X and Q bands is shown in figure 2 throughout the temperature range of the spin transition. The spectra only slightly change from room temperature down to 174 K (figure 2(a)), then a striking change occurs in the range 174–168 K (figures 2(b) and 2(c)). At lower temperatures the spectra remain almost temperature independent (figure 2(d)). In the warming mode a similar behaviour is observed: from 20

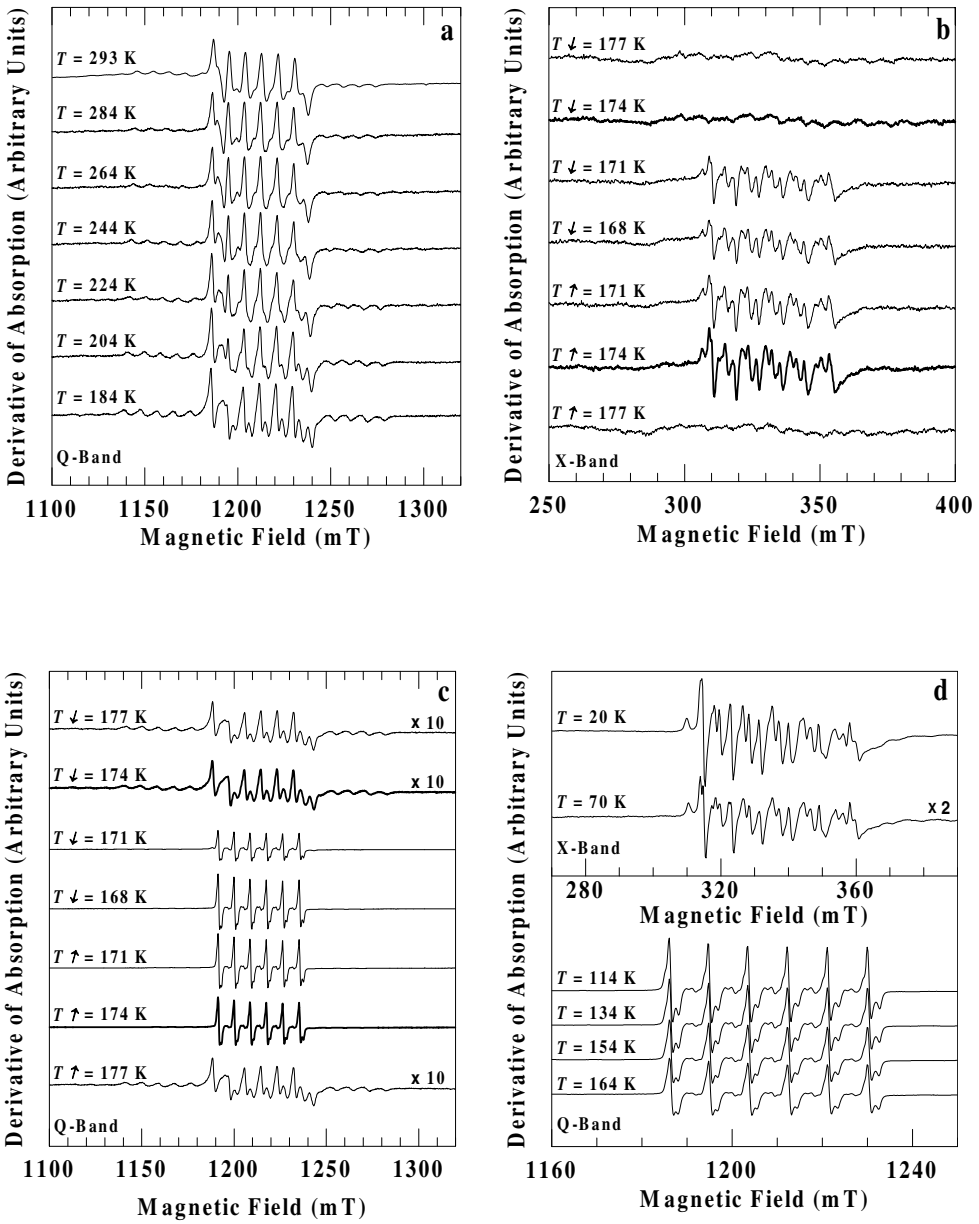

Figure 2. EPR spectra of $[Fe(PM\text{-}BiA)_2(NCS)_2]$ in powder form: (a) in Q band above the hysteresis loop; (b) in X band and (c) in Q band, in the cooling ($T_\downarrow$) and in the warming ($T_\uparrow$) modes in the vicinity of the hysteresis loop; (d) in X (top) and Q bands (bottom) below the hysteresis loop.

to 171 K the spectra do not significantly change, around 171–177 K a marked transformation takes place and at higher temperatures the EPR spectra vary very gradually.

All the spectra observed are typical of Mn^{2+} ions in a powder system and can be well described by the orthorhombic spin Hamiltonian including only quadratic zfs terms [26]:

$$\mathcal{H} = g\beta \boldsymbol{B}\cdot\boldsymbol{S} + D[S_z^2 - \tfrac{1}{3}S(S+1)] + E\left(S_x^2 - S_y^2\right) + A\boldsymbol{S}\cdot\boldsymbol{I} \qquad (2)$$

where $S = 5/2$ and $I = 5/2$, and all symbols have their usual meaning. The g-factor and the hfs constant A are isotropic with a good accuracy. Quite convincing fits to the experimental EPR spectra have been obtained neglecting such terms as the quartic zfs terms, as well as the nuclear Zeeman and nuclear quadrupole terms. So, these terms have been omitted from equation (2).

In the case of spectra occurring in the vicinity of the effective g-value $g_{eff} = 2.0$ the condition $|D|$, $|E|$, $|A| \ll g\beta B$ holds (the parameters D and E are defined with the usual convention that $0 \leqslant \eta = 3E/D \leqslant 1$). The presence in equation (2) of the zfs terms gives rise to five 'allowed' zfs multiplets, $\langle M-1, m| \leftrightarrow \langle M, m+\Delta m|$, $M = -S+1, \ldots, S$, $m = -I, \ldots, I$. Meanwhile, for comparable absolute values of zfs and hfs parameters, the selection rules governing the intensities of various hfs transitions are broken down, so that each zfs multiplet, besides six 'allowed' hfs components with $\Delta m = 0$, features a number of 'forbidden' hfs components with, $\Delta m \pm 1, \pm 2, \ldots, \pm 5$, $|m + \Delta m| \leqslant I$, their intensities dropping with the increase of Δm.

In order to obtain a quantitative characterization of the EPR spectra transformations throughout the whole temperature range studied, including the spin transition region, computer simulations have been carried out. Our laboratory-developed simulation program takes into account all 'allowed' zfs and 'allowed' and 'forbidden' hfs components. Their intensities are determined using the Bir method [27]. The resonance fields are calculated to third order in perturbation theory [10]. The EPR spectrum is computed as [26]

$$\mathcal{P}(B) = \sum_{M=-S+1}^{S} \sum_{m=-I}^{I} \sum_{\substack{\Delta m=0 \\ |m+\Delta m| \leqslant I}}^{5} \int_0^{2\pi} \int_0^{\pi} W(D, E, \vartheta, \varphi) \left| \frac{\mathrm{d}B_r}{\mathrm{d}\nu} \right| \times F[B - B_r(D, E, \vartheta, \varphi), \Delta B] \sin\vartheta \, \mathrm{d}\vartheta \, \mathrm{d}\varphi \tag{3}$$

where $W(D, E, \vartheta, \varphi)$ is the transition intensity averaged over all directions of the microwave magnetic field and F is the lineshape with an orientation-dependent linewidth ΔB, including broadening due to spin–lattice and spin–spin interactions as well as to static disorder, ϑ and φ are the polar and azimuthal angles of the static magnetic field $\boldsymbol{B}$ with respect to the axes of the spin Hamiltonian (2), $B_r(D, E, \vartheta, \varphi)$ is the resonance magnetic field, and ν is the microwave frequency.

Figure 3 shows the computer fits to the experimental EPR spectra of Mn^{2+}, in the LS state of Fe^{2+} (in the X and Q bands) and in the HS state of Fe^{2+} (in the Q band). Due to very close fits obtained in the two bands, the spin Hamiltonian parameters could be determined with a good accuracy. The g- and A-values are found as

$$g = 2.000 \pm 0.003 \qquad \text{and} \qquad A = (-82 \pm 1)10^{-4}\ \mathrm{cm}^{-1}.$$

These values are not appreciably modified in the course of the spin transition. In contrast, quite significant changes occur in the zfs parameters and in the intrinsic (Lorentzian) linewidth ΔB, see figures 4 and 5. Table 2 summarizes the best-fit EPR parameters at different temperatures.

3.3. Superposition model analysis

Generally, the change in the zfs parameter D produced by a change in temperature can be due to (i) structural transformations, (ii) thermal expansion of the crystal lattice and (iii) lattice vibrations. In a given spin state the variation with temperature of the D-values can be expressed as a sum

$$D(T) = D_s(T) + D_v(T) \tag{4}$$

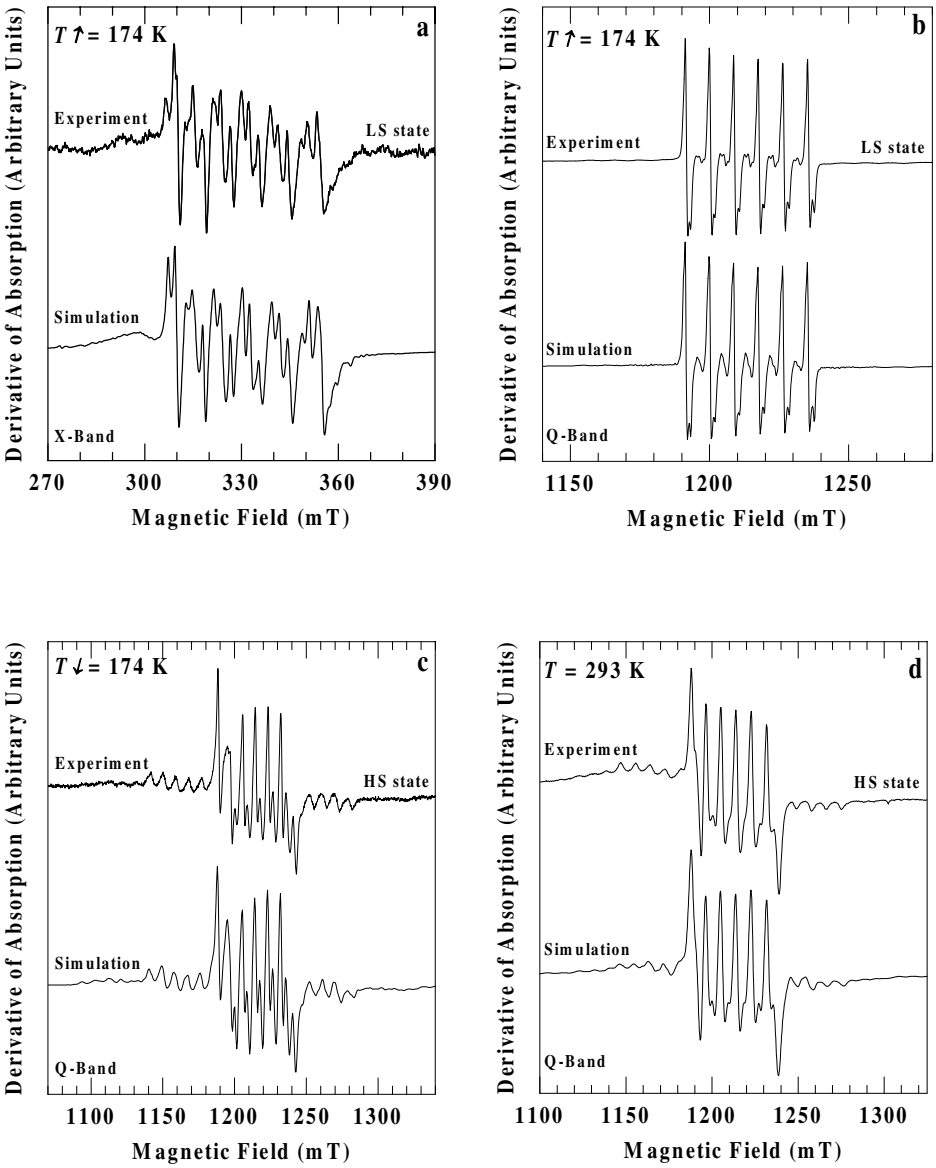

Figure 3. Computer simulations of the EPR spectrum of $[Fe(PM\text{-}BiA)_2(NCS)_2]$ in the LS state of Fe^{2+} ((a) X band and (b) Q band) and at two different temperatures in the HS state of Fe^{2+} ((c) and (d)). The measurement temperatures are indicated on the graphs. See table 2 for the simulation parameters.

where $D_s(T)$ is a contribution due to temperature expansion of the bond lengths and $D_v(T)$ arises from the lattice vibrations. The latter contribution is usually chosen in the form [32]

$$D_v(T) = D_{v0}\coth(\Theta/2T) \tag{5}$$

where D_{v0} is proportional to the fundamental phonon frequency at $T = 0\ K$ and Θ is the Debye temperature. It has been shown that this form gives a good description of the contribution of the lattice vibrations to the zfs parameters [33].

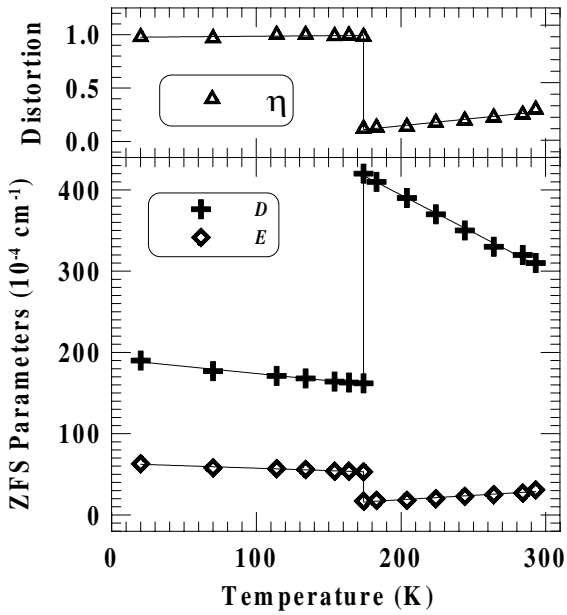

Figure 4. Temperature dependence of the best-fit zfs parameters for Mn^{2+} ions (symbols). The full curves are guides for the eyes.

The phenomenological superposition model [22, 28–31] provides a simple way of relating the D_s zfs parameter to the structure of environment of S-state ions, e.g. Mn^{2+}. In this model, the zfs parameters are expressed as sums of contributions from different ligands. For an arbitrarily distorted coordination polyhedron of the paramagnetic ion the components of the zfs tensor D'_{mn} in an arbitrary axis system x', y', z' can be written as [30]

$$D'_{mn} = \sum_{j=1}^{k} \bar{b}_2(r_j) K_{mn}(\vartheta_j, \varphi_j) \tag{6}$$

where the subscript j runs over the k ligands with spherical coordinates, r_j, ϑ_j and φ_j. In equation (6) $\bar{b}_2(r_j)$ are radial functions, and the coordination factors $K_{mn}(\vartheta_j, \varphi_j)$, where m, $n = x', y', z'$, are explicit functions of the angular positions of the ligands:

$$K_{mn}(\vartheta_j, \varphi_j) = 3(l^j_m l^j_n - \tfrac{1}{3}\delta_{mn}) \tag{7}$$

where l^j_m are the directional cosines of the jth ligand, $l^j_{x'} = \sin\vartheta_j \cos\varphi_j$, $l^i_{y'} = \sin\vartheta_j \sin\varphi_j$, $l^j_{z'} = \cos\vartheta_j$ and δ_{mn} are the Kronecker symbols. The values of D and E are obtained by diagonalizing the D'_{mn} matrix and putting down

$$D = \tfrac{3}{2}D_z \qquad \text{and} \qquad E = \tfrac{1}{2}(D_x - D_y) \tag{8}$$

where the non-primed single-subscript D_n values refer to the principal axis system. Last, by permuting the x, y, z axes, D and E are expressed in the standard axis system with $0 \leqslant \eta = 3E/D \leqslant 1$ (see above).

The radial functions $\bar{b}_2(r_j)$ are most often taken in the form [28–31]

$$\bar{b}_2(r_j) = \bar{b}_2(r_0)\left(\frac{r_0}{r_j}\right)^{t_2} \tag{9}$$

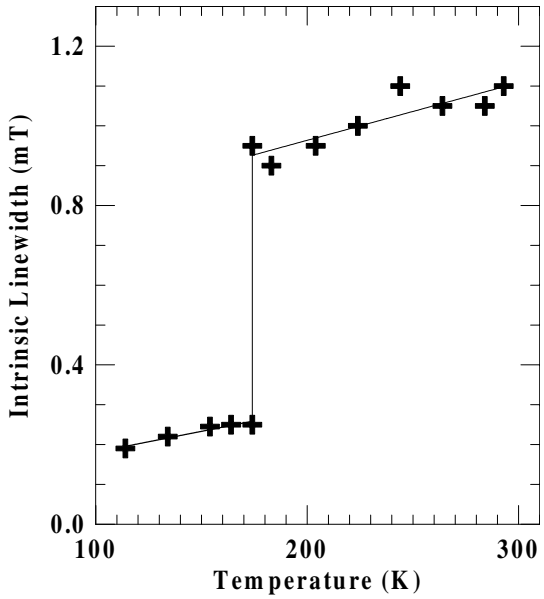

Figure 5. Temperature dependence of the intrinsic Lorentzian EPR linewidth ΔB (symbols), determined by computer simulations of the Q-band spectra, see equation (3). The full curve is a guide for the eyes.

Table 2. Best-fit EPR parameters for Mn^{2+} ions in $[Fe(PM\text{-}BiA)_2(NCS)_2]$ at different temperatures. The 20 and 70 K data have been obtained in the X band, and the remaining ones in the Q band. The numbers in parentheses are the standard errors in the last digit estimated by means of trial simulation with parameter values slightly different from their best-fit values.

T (K)	Fe^{2+} spin state	D (10^{-4} cm^{-1})	E (10^{-4} cm^{-1})	$\eta = 3E/D$	ΔB (mT)
20	LS	190(5)	63(3)	0.99(2)	0.25(5)
70	LS	177(5)	58(3)	0.98(2)	0.30(5)
114	LS	171(5)	57(3)	1.00(2)	0.19(5)
134	LS	168(5)	56(3)	1.00(2)	0.22(5)
154	LS	164(5)	54(3)	0.99(2)	0.24(5)
164	LS	163(5)	54(3)	0.99(2)	0.25(5)
$T_\uparrow = 174$ K	LS	162(5)	53(3)	0.98(2)	0.25(5)
$T_\downarrow = 174$ K	HS	420(5)	17(3)	0.12(2)	0.95(5)
183	HS	410(5)	18(3)	0.13(2)	0.90(5)
204	HS	390(5)	18(3)	0.14(2)	0.95(5)
224	HS	370(5)	20(3)	0.16(2)	1.00(5)
244	HS	350(5)	23(3)	0.20(2)	1.10(5)
264	HS	330(5)	25(3)	0.23(2)	1.05(5)
284	HS	320(5)	27(3)	0.25(2)	1.05(5)
293	HS	310(5)	31(3)	0.30(2)	1.10(5)

where $\bar{b}_2(r_0)$ is an intrinsic parameter depending on the mean bond length between the paramagnetic ion and the ligands, r_0, and t_2 is a power-law exponent. In this model $\bar{b}_2(r_0)$ and t_2 are treated as adjustable parameters. For Mn^{2+} t_2 usually is taken as 7 ± 1 [28, 29], although a value twice as large, $t_2 = 14$, has also been inferred [31]. Equation (9) is sometimes

Table 3. Projections of the Fe–N_j bond lengths in the x/a, y/b and z/c unit cell system, respectively, Δa_i; Δa_j, Δb_i; Δb_j and Δc_i; Δc_j, in the two spin states of Fe^{2+}. The three pairs of subscripts (i, j) correspond to three pairs of equivalent nitrogen atoms, see text. The numbers in parentheses are the standard errors in the last digit.

	LS	HS
Δa_1; Δa_2	0.040 25(2)	0.050 93(2)
Δb_i; Δb_2	0.084 84(2)	0.087 61(2)
Δc_1; Δc_2	0.076 22(2)	0.079 52(2)
Δa_3; Δa_4	0.145 51(2)	0.161 21(2)
Δb_3; Δb_4	0.052 84(2)	0.047 26(2)
Δc_3; Δc_4	0.005 40(2)	0.017 81(2)
Δa_5; Δa_6	0.024 57(2)	0.007 96(2)
Δb_5; Δb_6	0.088 91(2)	0.093 61(2)
Δc_5; Δc_6	0.078 25(2)	0.098 93(2)

considered as a power-law approximation of the Lennard-Jones type potential, e.g. see [28]:

$$\bar{b}_2(r_j) = -A\left(\frac{r_0}{r_j}\right)^p + B\left(\frac{r_0}{r_j}\right)^q. \tag{10}$$

The superposition model has been widely used in the analysis of the spin Hamiltonian parameters of the ^{6}S-state ions with oxygen or fluorine ligands. Meanwhile, to our knowledge, no attempt has been made to apply this model to the Mn^{2+} ion in a nitrogen environment.

In order to apply the superposition model to the present case, the following assumptions have been made.

(i) We assume the Mn^{2+} probe to substitute for Fe^{2+}. Indeed, the Mn^{2+} ion is known to prefer sixfold coordinated sites, occupied by Fe^{2+} in the structure of $[Fe(PM\text{-}BiA)_2(NCS)_2]$.

(ii) In the LS state the environment of Fe^{2+} is supposed to be temperature independent with respect to the unit cell system. Indeed, the crystal structure data show that in the x/a, y/b and z/c unit cell system the Fe–N bond lengths and N–Fe–N angles are almost the same at 140 and 25 K.

(iii) In the HS state the bond angles are supposed to be temperature independent, as suggested by the linear temperature dependence of the unit cell parameters.

(iv) We allow for a linear thermal expansion of the bond lengths between the metal ion and the jth ligand in proportion to the temperature expansion of the unit cell parameters:

$$r_j(T) = \sqrt{(\Delta a_j a(T))^2 + (\Delta b_j b(T))^2 + (\Delta c_j c(T))^2} \tag{11}$$

where Δa_j, Δb_j, Δc_j are projections of the Fe–N_j bonds on the respective axes of the unit cell system listed in table 3. This $r_j(T)$ dependence is then inserted in equation (9) in order to account for $D_s(T)$ in equation (4).

The adjustable parameters of the present model taking into account both the thermal expansion and lattice vibrations are $\bar{b}_2(r_0)$, t_2, D_{v0} and Θ. For the reference radial distance the value of $r_0 = 2.101$ Å has been chosen [29].

With such a number of adjustable parameters, some additional assumptions are necessary. We have somewhat arbitrarily assumed that D_{v0} and Θ in equation (5) do not change in the spin transition. In this case, the fitting to the experimental temperature dependence of D yields $D_{v0} = -80 \times 10^{-4}$ cm^{-1} and $\Theta = 500$ K.

As far as the true metal-to-ligand distances are concerned, we note that in the sixfold coordination the ionic radius of the substituting spin probe Mn^{2+}, $R_{Mn^{2+}} = 0.97$ Å, is

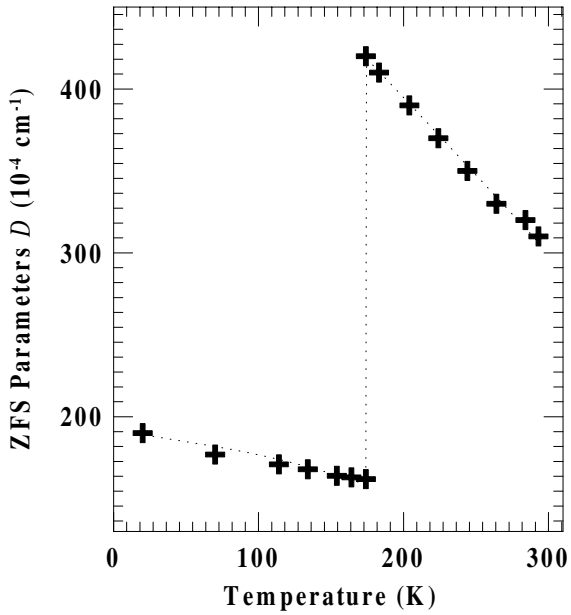

Figure 6. Computer fit (dashed curve) to the temperature dependence of the zfs parameter D (symbols) versus temperature (for $x = 0$). See text for details.

considerably different from those of the replaced Fe^{2+} ion in both the LS and HS states, respectively $R_{Fe^{2+}_{LS}} = 0.75$ and $R_{Fe^{2+}_{HS}} = 0.92$ Å [34]. Therefore, in the environment of Mn^{2+} the arrangement of the ligands can be somewhat different from that in the host crystal (with respect to the Fe^{2+} ions). In particular, the change of the metal-to-ligand distances at the spin conversion temperature is certainly less pronounced for Mn^{2+}, since this ion does not undergo any transition at this temperature. In this context, we have computer fitted the experimental temperature dependence of the zfs parameter D for Mn^{2+} ions with metal-to-ligand distances chosen in accordance with the following expressions:

$$\text{in the LS state } r_j(T) = d_{Mn^{2+}-N_j} = d_{Fe^{2+}_{LS}-N_j} + x(R_{Mn^{2+}} - R_{Fe^{2+}_{LS}}) \tag{12}$$

$$\text{in the HS state } r_j(T) = d_{Mn^{2+}-N_j} = d_{Fe^{2+}_{HS}-N_j} + x(R_{Mn^{2+}} - R_{Fe^{2+}_{HS}}) \tag{13}$$

with x-values quoted in table 4.

In particular, for the $x = 0$ choice any possible modifications of the bond lengths caused by the substitution of Fe^{2+} by Mn^{2+} are neglected. Figure 6 shows the results of the corresponding computer fit to the temperature dependence of D for Mn^{2+} in the whole temperature range of this study, including both the LS and HS states of Fe^{2+} ions. The best-fit parameters determined in this case are as follows:

$$\text{in the LS state } \bar{b}_2(r_0) = -0.0165 \text{ cm}^{-1} \text{ and } t_2 = 4$$

$$\text{in the HS state } \bar{b}_2(r_0) = -0.0245 \text{ cm}^{-1} \text{ and } t_2 = 8.$$

Another choice of the x-value results only in a linear change of the $\bar{b}_r(r_0)$-parameter versus the metal-to-ligand distances, see table 4.

Table 4. Best fit values of the superposition model parameter $\bar{b}_2(r_0)$ for different metal-to-ligand distances, see equations (12) and (13). The numbers in parentheses are the standard errors in the last digit.

	$\bar{b}_2(r_0)$ (cm^{-1})	
x	LS state	HS state
0	−0.0165(5)	−0.0245(5)
0.25	−0.0185(5)	−0.0255(5)
0.5	−0.0205(5)	−0.0270(5)
0.75	−0.0225(5)	−0.0285(5)
1	−0.0255(5)	−0.0300(5)

4. Discussion

4.1. Mn^{2+} as a probe of the spin transition

In EPR studies of ferrous spin-crossover compounds a marked line broadening is always observed at the spin transition temperature, due to the advent of paramagnetic HS Fe^{2+} ions. However, in the present instance, see figure 5, this broadening is very moderate in comparison with that previously reported for triazole compounds [19, 20], so that the Q-band Mn^{2+} EPR spectra remain quite well resolved not only in the LS state but also in the HS state of Fe^{2+}. One can conclude that EPR is certainly much better adapted to the study of the spin transitions in molecular crystals in which the distance between spin changing ions is much larger that in polymeric triazole-based compounds.

Note also a net improvement of spectra resolution in the Q-band spectra in comparison with the X-band ones, see figure 2. In the X-band spectra corresponding to the LS state of Fe^{2+} ($T_{\downarrow} = 171$ K to $T_{\uparrow} = 174$ K) only the hfs components of the central zfs multiplet, $\langle -1/2, m| \leftrightarrow \langle +1/2, m + \Delta m|$, are resolved. In the HS state of Fe^{2+} the resolution in this part of the spectrum is partly lost; however, some new, relatively broad, peaks appear an higher and lower magnetic fields, indicating an increase of the zfs parameters, see figure 2(b). In contrast, in the Q band a quite well resolved EPR spectrum is observed even when all Fe^{2+} ions are in the HS state, see figures 2(a) and 2(c). The improvement of resolution in the Q-band spectra B_r in the present instance is readily explained by the structure of the resonance magnetic field expression. Indeed, for the *central* zfs multiplet the dependence of B_r on the zfs parameters contains only perturbation terms in $D/g\beta B_r$ and $E/g\beta B_r$ [10]. As the apparent width of the resonance features in a powder EPR spectrum is due mainly to angular variations of B_r, in passing from the X to the Q band these features are narrowed approximately in proportion to the ratio of B_r-values for the two bands.

From an inspection of the best-fit zfs parameter values for Mn^{2+} ions, see table 2, one can conclude that D, E and $\eta = 3E/D$ are considerably modified in the course of the spin transition of Fe^{2+}. Thus, significant structural transformations arise not only in the close environment of Fe^{2+} but also in the environment of the spin probe. In the LS state of Fe^{2+}, the maximal degree of rhombic distortion is attained, $\eta \approx 1$. In the HS state of Fe^{2+}, in the vicinity of the spin transition (at $T_{1/2\downarrow} = 174$ K) the symmetry is quasi-axial with $\eta \approx 0.12$. At higher temperatures the orthorhombic distortion increases up to $\eta \approx 0.3$ at 293 K. Note that inside the hysteresis loop at the same temperature (174 K) the axial zfs parameter D is almost three times larger in the HS state than in the LS state of Fe^{2+}. This indicates a relatively strong axial distortion arising at the Mn^{2+} sites in the HS state of Fe^{2+} ions.

4.2. Structural inferences

In applying the superposition model to the zfs parameter D of Mn^{2+}, the power law exponent t_2 turns out to be insensitive to the choice of the metal-to-ligand distances. On the other hand, we have verified that the temperature dependence of the D-values cannot be fitted with a single Lennard-Jones potential, equation (10), with one and the same set of A-, B-, p-, and q-values. This is consistent with the fact that a considerable structural change occurs in the course of the spin transition.

On the basis of equations (9) and (10), large and positive t_2-values in the power-law approximation of the Lennard-Jones potential are expected for a relatively loose fit when the host ion is larger that the substituting spin probe; in the opposite case of a tight fit small (or even negative) t_2 would rather be observed [22]. In the present instance, the t_2-values found in the two spin states of Fe^{2+} are in agreement with this tendency, as far as the mismatch between its ionic radii and that of the spin probe is more pronounced in the LS state. Moreover, the large foreign Mn^{2+} ions tend to push out the ligands, so that equilibrium Mn–N bond lengths are probably less different from each other than the corresponding Fe–N bond lengths.

It is worth noting that the crystallographic data indicate a more regular arrangement of the FeN_6 core in the LS state than in the HS state. In contrast, the EPR data show that the coordination polyhedra of manganese do not follow this trend: while the axial zfs parameter D is lowered, the rhombic zfs parameter is markedly increased in the LS state of Fe^{2+}. These low-symmetry distortions are probably due to slightly different angular positions of ligands in the case of Mn^{2+} and Fe^{2+} ions. However, in the case of S ions the zfs parameter values are related to contributions of excited states of these ions, which may have different signs. Therefore, a small variation of crystal field can bring about a large contribution to the zfs parameters.

5. Conclusion

In the $[Fe(PM\text{-}BiA)_2(NCS)_2]$ molecular compound the Mn^{2+} EPR spectra undergo a striking transformation in the temperature range of the spin transition experienced by the Fe^{2+} ions. From the viewpoint of EPR spectroscopy, molecular compounds, in comparison with the triazole-based polymeric spin-transition compounds previously investigated by EPR, have the advantage of being magnetically more diluted. Therefore, the intrinsic linewidth of the Mn^{2+} spin probe remains reasonably small even when all the Fe^{2+} ions are in the HS state, so that the EPR can provide significant data on the crystal structures both below and above the spin transition.

Computer simulations clearly show that the transformation of the EPR spectra in the course of the spin transition are mainly due to the change in the zero-field splitting parameters. It can be concluded that, on the short-range order scale, the spin transition of Fe^{2+} induces considerable modifications not only in its own close environment but also in the whole crystal structure including the close environment of the spin probe. This means that a considerable cooperativity exists between the metal ions.

The EPR data show quite comparable low-symmetry distortions in the environment of the Mn^{2+} probe in both spin states of the Fe^{2+} ions. One can infer that the departure from cubic symmetry of environment of the Mn^{2+} ions is mainly caused by angular distortions.

In spite of a considerable uncertainty persisting with regard to the interatomic distances between the Mn^{2+} spin probe and its ligands, a quite consistent result is obtained concerning the reduction in the LS state of Fe^{2+} of the power law exponent t_2. This tendency is in agreement with the fact that the Mn^{2+} ions are more tightly fitted to the less roomy LS Fe^{2+} sites in comparison with the HS Fe^{2+} sites.

References

[1] Kahn O 1993 *Molecular Magnetism* (New York: VCH)
[2] Gütlich P, Hauser A and Spiering H 1994 *Angew. Chem. Int. Edn Engl.* **33** 2024
[3] Kahn O, Kröber J and Jay C 1992 *Adv. Mater.* **4** 718
[4] Jay C, Groliere F, Kahn O and Kröber J 1993 *Mol. Cryst. Liq. Cryst.* **234** 255
[5] Létard J-F, Montant S, Guionneau P, Martin P, Le Calvez A, Freysz E, Chasseau D, Lapouyade R and Kahn O 1997 *J. Chem. Soc. Chem. Commun.* 745
[6] Gaudry J-B, Capes L, Langot P, Létard J-F, Lavastre O, Freysz E and Kahn O *Chem. Phys. Lett.* submitted
[7] Létard J-F, Guionneau P, Codjovi E, Lavastre O, Bravic G, Chasseau D and Kahn O 1997 *J. Am. Chem. Soc.* **119** 10 861
[8] Létard J-F, Guionneau P, Rabardel L, Howard J A K, Goeta A E, Chasseau D and Kahn O 1998 *Inorg. Chem.* **37** 4432
[9] Guionneau P, Létard J-F, Yufit D S, Chasseau D, Bravic G, Goeta A E, Howard J A K and Kahn O 1999 *J. Mater. Chem.* **9** 985
[10] Daubric H, Cantin C, Thomas C, Kliava J, Létard J-F and Kahn O 1999 *Chem. Phys.* **244** 75
[11] Rao P S, Reuveni A, McGarvey B R, Ganguli P and Gütlich P 1981 *Inorg. Chem.* **20** 204
[12] Ozarowski A and McGarvey B R 1989 *Inorg. Chem.* **28** 2262
[13] Doan P E and McGarvey B R 1990 *Inorg. Chem.* **29** 874
[14] Vreugdenhil W, Van Diemen J H, De Graaff R A G, Hassnoot J G and Reedijk J 1990 *Polyhedron* **9** 2971
[15] Ozarowski A, Shunzhong Y, McGarvey B R, Mislankar A and Drake J E 1991 *Inorg. Chem.* **30** 3167
[16] Cantin C, Daubric H, Kliava J, Servant Y, Sommier L and Kahn O 1998 *J. Phys.: Condens. Matter* **10** 7057
[17] Cantin C, Daubric H, Kliava J and Kahn O 1998 *Solid State Commun.* **108** 17
[18] Létard J-F, Daubric H, Cantin C, Kliava J, Bouhedja Y A, Nguyen O and Kahn O 1999 *Mol. Cryst. Liq. Cryst.* **335** 1207
[19] Cantin C, Kliava J, Servant Y, Sommier L and Kahn O 1997 *Appl. Magn. Reson.* **12** 81
[20] Cantin C, Kliava J, Servant Y, Sommier L and Kahn O 1997 *Appl. Magn. Reson.* **12** 87
[21] Sung R C W and McGarvey B R 1999 *Inorg. Chem.* **38** 3644
[22] Newman D J 1971 *Adv. Phys.* **21** 197
[23] Real J A, Gallois B, Granier T, Suez-Panama F and Zarembovitch J 1992 *Inorg. Chem.* **31** 4972
[24] Guionneau P, Kepert C J, Rosseinsky M, Chasseau D, Gaultier J, Kurmoo M, Hursthouse M B and Day P 1998 *J. Mater. Chem.* **8** 367
[25] Gaultier J, Hébrard-Brachetti S, Guionneau P, Kepert C J, Chasseau D, Ducasse L, Barrans Y, Kurmoo M and Day P 1999 *J. Solid State Chem.* **145** 496
[26] Kliava J 1986 *Phys. Status Solidi* b **134** 411
[27] Bir G L 1964 *Sov. Phys.–Solid State* **5** 1628
[28] Newman D J and Urban W 1976 *Adv. Phys.* **9** 793
[29] Newman D J and Siegel E 1976 *J. Phys. C: Solid State Phys.* **9** 4285
[30] Kliava J 1982 *J. Phys. C: Solid State Phys.* **15** 7017
[31] Yu W-L and Zhao M-G 1988 *Phys. Rev.* B **37** 9254
[32] Leclerc A and Manoogian A 1975 *J. Chem. Phys.* **63** 4456
[33] Gleason R J, Boldú J L, Cabrera E, Quintanar C and Muñoz P E 1997 *J. Phys. Chem. Solids* **58** 1507
[34] Shannon R D 1976 *Acta Crystallogr.* A **32** 751